Cone Structure in Retinal Degeneration Associated with Mutations in the *peripherin/RDS* Gene

Jacque L. Duncan,[1] Katherine E. Talcott,[1] Kavitha Ratnam,[1] Sanna M. Sundquist,[1] Anya S. Lucero,[1] Shelley Day,[1] Yuhua Zhang,[2,3] and Austin Roorda[2]

PURPOSE. To study cone photoreceptor structure and function associated with mutations in the second intradiscal loop region of *peripherin/RDS*.

METHODS. High-resolution macular images were obtained with adaptive optics scanning laser ophthalmoscopy and spectral domain optical coherence tomography in four patients with *peripherin/RDS* mutations and 27 age-similar healthy subjects. Measures of retinal structure and fundus autofluorescence (AF) were correlated with visual function, including best-corrected visual acuity (BCVA), kinetic and static perimetry, fundus-guided microperimetry, full-field electroretinography (ERG), and multifocal ERG. The coding regions of the *peripherin/RDS* gene were sequenced in each patient.

RESULTS. Heterozygous mutations in *peripherin/RDS* were predicted to affect protein structure in the second intradiscal domain in each patient (Arg172Trp, Gly208Asp, Pro210Arg and Cys213Tyr). BCVA was at least 20/32 in the study eye of each patient. Diffuse cone-greater-than-rod dysfunction was present in patient 1, while rod-greater-than-cone dysfunction was present in patient 4; macular outer retinal dysfunction was present in all patients. Macular AF was heterogeneous, and the photoreceptor-retinal pigment epithelial (RPE) junction layer showed increased reflectivity at the fovea in all patients except patient 1, who showed cone-rod dystrophy. Cone packing was irregular, and cone spacing was significantly increased (z-scores >2) at most locations throughout the central 4° in each patient.

CONCLUSIONS. *peripherin/RDS* mutations produced diffuse AF abnormalities, disruption of the photoreceptor/RPE junction, and increased cone spacing, consistent with cone loss in the macula. The abnormalities observed suggest that the integrity of the second intradiscal domain of peripherin/RDS is critical for normal macular cone structure. (*Invest Ophthalmol Vis Sci.* 2011;52:1557–1566) DOI:10.1167/iovs.10-6549

Peripherin/RDS is an integral membrane glycoprotein involved in photoreceptor outer segment formation.[1] *peripherin/RDS* mutations on chromosome 6p were first reported to cause autosomal dominant retinitis pigmentosa (RP)[2,3] but have since been shown to cause a wide variety of retinal phenotypes including pattern dystrophy,[4,5] cone-rod dystrophy,[6] adult vitelliform macular dystrophy,[7] central areolar choroidal dystrophy,[8,9] and autosomal dominant macular dystrophy.[10] Peripherin/RDS forms a complex with ROM1, which also plays a role in photoreceptor outer segment disc formation, and heterozygous mutations in *peripherin/RDS* and *ROM1* may produce a digenic form of RP.[11]

The highly conserved second intradiscal loop is thought to be integral for peripherin/RDS protein function and, thus, for outer segment disc generation and stabilization.[6,12] More than 90 different mutations in the *peripherin/RDS* gene have been associated with retinal degeneration, and mutations at the same amino acid position have been associated with diverse clinical phenotypes (http://www.retina-international.org/sci-news/rdsmut.htm). Mutations affecting the intradiscal D2 domain of peripherin/RDS manifest a variety of different retinal degeneration phenotypes, supporting the importance of this region for normal photoreceptor outer segment structure and survival. Altering the DNA from cysteine to thymidine at position 514 of the *peripherin/RDS* cDNA causes an arginine to tryptophan substitution at position 172 (R172W), which has been associated with macular dystrophy, central areolar choroidal dystrophy, cone dystrophy, and cone rod dystrophy.[6,10,13–23] Changing guanine to adenosine at position 623 alters the amino acid at position 208 from glycine to aspartic acid (G208D) and is thought to alter the secondary structure of the protein.[24] The G208D mutation has been associated with atypical autosomal dominant RP,[25] pattern macular dystrophy,[10] and central areolar dystrophy.[13] Substituting guanine for cysteine at position 629 changes the amino acid at position 210 from proline to arginine (P210R)[23,26] and produces adult foveomacular dystrophy[26] and both macular and peripheral retinal degeneration, including cone-rod degeneration and RP.[23,27] Finally, substituting guanine for adenosine at position 637 changes the amino acid at position 213 from cysteine to tyrosine and causes pattern dystrophy.[4] This cysteine is thought to play an important role in intrachain or interchain disulfide bond formation, and mutations at this location may disrupt photoreceptor disc membrane integrity, resulting in photoreceptor degeneration and lipofuscin accumulation in RPE cells.[4]

Given the dramatic phenotypic variation observed within and between families with the same mutation, the effect of peripherin/RDS mutations on cone structure in living eyes is

TABLE 1. Summary of Retinal Functional and Structural Testing

Patient	Age (y)	Genotype	Eye	BCVA	ETDRS Score	Foveal Threshold (dB)	Color Vision*	Automated Perimetry	Kinetic Perimetry
1	45	Heterozygous c.637C>A (Cys213Tyr)	OD	20/20	83	32	0; 1.00	Dense ring scotoma beginning at 6° eccentric to fixation bilaterally	Inferonasal scotoma from 5°–20° to I4e target bilaterally
			OS	20/20	84	35	56; 1.39		
2	49	Heterozygous c.514C>T (Arg172Trp)	OD	20/20	85	32	255; 2.18	Dense ring scotoma extending from 3°–10° eccentric to fixation bilaterally	Full to V4e, 30° central scotoma to I4e bilaterally
			OS	20/20	85	26	344.5; 2.94		
3	60	Heterozygous c.623G>A (Gly208Asp)	OD	20/20	85	35	259.4; 2.22	Dense ring scotoma extending 4°–8° eccentric to fixation bilaterally	Full to V4e, 35° central scotoma to I4e bilaterally
			OS	20/25	80	34	283.6; 2.42		
4	65	Heterozygous c.629C>G (Pro210Arg)	OD	20/30	75	32	228.9; 1.96	Dense ring scotoma extending from 3°–10° eccentric to fixation	Dense ring scotoma 5°–30° to V4e and 2°–40° to I4e
			OS	5/100	35	13	Not tested		

ETDRS, early treatment of diabetic retinopathy visual acuity score, expressed as number of letters correctly identified; GVF, Goldmann visual field; mfERG, multifocal electroretinogram.

* Farnsworth D15 total color difference score (TCDS) and color confusion index (CCI; CCI = $TCDS_{patient}/TCDS_{normal}$) based on Bowman scoring method; normal = 1.00[39]; Lanthony desaturated D15 total error score and CCI are reported for patient 1, who made no errors on the Farnsworth D15 test[40]; CFS thickness (mean ± 1 SD) of 18 normal eyes aged 41 to 75 years = 286.4 ± 16.2 μm.

† Expressed as a percentage of the normal mean amplitude (rod, 272 μV; cone flicker, 121 μV); 2 SD below normal is 65% for rod b-wave and 54% for cone flicker; normal rod timing is <105 ms; normal cone flicker timing is <32 ms.

not clearly understood. Adaptive optics scanning laser ophthalmoscopy (AOSLO) uses adaptive optics to overcome optical imperfections in living eyes and can be used to obtain retinal images with lateral resolution of approximately 2 μm, allowing direct visualization of photoreceptors.[28–31] Direct visualization of the cone mosaic in patients with retinal degeneration allows comparison of cone spacing, density, and regularity with healthy subjects.[32–35] In combination with other imaging and diagnostic modalities, measures of cone structure provide insight into the effect different types of retinal degeneration have on macular cones.[32,33,36–38] Here we present high-resolution retinal images for four patients with mutations in the *peripherin/RDS* gene, allowing direct in vivo genotype-phenotype correlation of cone photoreceptor structure and function at the cellular level.

METHODS

Research procedures followed the tenets of the Declaration of Helsinki. Informed consent was obtained from all subjects after explanation of the nature and possible consequences of the studies. The study protocol was approved by the institutional review boards of the University of California at San Francisco and the University of California at Berkeley.

Clinical Examination

A complete history was obtained, including information about all known family members. Clinical findings are summarized in Table 1. Measurement of best-corrected visual acuity (BCVA) was performed using a standard eye chart according to the Early Treatment of Diabetic Retinopathy Study protocol. The eye with better visual acuity or more stable fixation, or both, was chosen for further study. Goldmann kinetic perimetry was performed with V-4e and I-4e targets. Automated perimetry was completed with a Humphrey visual field analyzer (HFA II 750-6116-12.6; Carl Zeiss Meditec, Inc., Dublin, CA) 10-2 SITA-standard threshold protocol with measurement of foveal thresholds, using a Goldmann III stimulus on a white background (31.5 apostilbs);

exposure duration was 200 ms. Color vision was examined using the Farnsworth Dichotomous Test for Color Blindness (D-15; Psychological Corporation, New York, NY); patient 1 made no errors on the Farnsworth D15 test and was tested using the Lanthony's Desaturated 15 Hue test. The data were analyzed using a Web-based platform scoring method (http://www.torok.info/colorvision), and the error scores were calculated using methods proposed by Bowman[39] and Lanthony.[40] Pupils were dilated with 1% tropicamide and 2.5% phenylephrine before obtaining optical coherence tomography (OCT), infrared SLO, and fundus autofluorescence (AF) images using a laser scanning system (Spectralis HRA + OCT Laser Scanning Camera System; Heidelberg Engineering, Vista, CA). The infrared beam of the super luminescent diode, center wavelength 870 nm, was used to acquire 20° horizontal scans through the locus of fixation; scans included 100 A-scans/B-scan for images through the locus of fixation and 10 A-scans/B-scan for the 19 horizontal scans used to acquire the 20° × 15° volume scans. Central foveal subfield (CFS) thickness, defined as the average of all points within the inner circle of 1-mm radius from a 20° volume scan with 19 raster lines separated by 266 μm, was measured using the laser scanning (Spectralis HRA + OCT Laser Scanning Camera System; Heidelberg Engineering) software. The software automatically maps the strongest two edges in each tomogram, one at the vitreoretinal interface and the other at the basement membrane of the retinal pigment epithelium (RPE)-Bruch membrane complex. CFS thickness of the study patients was compared with values from 18 normal eyes ranging in age from 41 to 75 years (normal, 286.4 ± 16.2 μm [mean ± 1 SD mean ± 1 SD =]). Full-field ERG was performed after 45 minutes of dark adaptation using a Burian-Allen contact lens electrode (Hansen Ophthalmic Development Laboratory, Iowa City, IA), according to International Society for Clinical Electrophysiology and Vision (ISCEV) standards[41] and as described previously.[33] Reduced amplitudes were reported as percentage below the mean; normal mean values and standard deviations (SD) are presented in Table 1. Multifocal ERG testing was performed in a light-adapted state (VERIS 5.1.10×; Electro-Diagnostic Imaging, Inc., Redwood City, CA), using a Burian-Allen contact lens electrode according to ISCEV standards, as previously described.[32,36] Fundus-guided microperimetry (MP-1; Nidek Technologies America Inc., Greensboro, NC) tested 45 locations

OCT CFS Thickness (μm)	Rod ERG b-Wave Amplitude† (μV)	Rod ERG b-Wave Timing (ms)	Cone ERG Flicker Amplitude† (μV)	Cone ERG Flicker Timing (ms)	mfERG
218	70.3	106	30	35.5	Severely reduced amplitude, delayed responses throughout central 40°, preserved central trace
233	107.3	105.5	25	35.5	
237	396.1	74.5	102.2	28.4	Severely reduced responses with delayed timing throughout central 15°, preserved peripheral responses
Not imaged	373.8	76.5	106.9	27.6	
221	254.5	93.5	59.9	30.6	Severely reduced amplitude, delayed responses in ring from 5°–15°, preserved central trace
217	200.1	103.5	60.4	30.4	
231	Not measurable	Not measurable	21.5	38	Severely reduced amplitude, delayed responses throughout central 40°, preserved central trace
197	Not measurable	Not measurable	18.8	36.5	

within the central 8° visual field, as previously described.[32,33,36] Numeric sensitivities in decibels (dB) were exported and overlaid with AOSLO images using computing software (MatLab; The MathWorks, Natick, MA). Mean ± 1 SD normal values across the central 10° for subjects aged 21 to 40 were 19.5 ± 1.1 dB (Midena et al., *IOVS* 2006;47:ARVO E-Abstract 5349).

Genetic Testing

Molecular analysis of the *peripherin/RDS* gene was performed by CLIA-certified laboratories (John and Marcia Carver Nonprofit Genetic Testing Laboratory, Iowa City, IA; University of Michigan Ophthalmic Molecular Diagnostic Laboratory, Ann Arbor, MI; University of Texas-Houston Laboratory for the Molecular Diagnosis of Inherited Eye Disease, Houston, TX, through eyeGENE). The three coding exons and the flanking intronic regions of the peripherin/RDS gene were amplified by PCR and sequenced in two directions. The NCBI Reference Sequence Data Project (RefSeq; http://www.ncbi.nlm.nih.gov/refseq/) reference mRNA sequence is NM_000322, with codon 1 corresponding to the start ATG and nucleotide 1 corresponding to the A.

AOSLO Image Acquisition and Cone Spacing Analysis

High-resolution images were obtained using AOSLO, and images were analyzed with customized software to determine cone spacing measures using previously described methods.[32,33,36,42] Cone spacing measures were compared with those of 27 healthy subjects ranging in age from 20 to 72. The average number of measurements per healthy subject was more than eight; no more than 15 measures were taken for any person. A double exponential function was fit to the spacing data:

$$\text{Cone spacing} = Ae^{(-C \times \text{eccentricity})} + Be^{(-D \times \text{eccentricity})}$$

where A, B, C and D are constants; 95% confidence limits were estimated using the curve-fitting toolbox (MatLab; The MathWorks). Cone spacing in the patients was measured at a range of eccentricities from as close to the fovea as possible out to 5° eccentricity in all

directions. Z-scores for each patient's cone spacing measurements were computed as the number of standard deviations from the best-fitting line to the normal data.

The exact location of the retina used for fixation (preferred retinal locus [PRL]) was determined by recording a video while the patient looked at a target that was delivered through modulation of the AOSLO scanning raster. As such, the fixation target was encoded into the video, and the region of the retina used to fixate the target could be determined using custom image analysis tools (MatLab; The MathWorks).

To further quantify the differences in eyes between patients and subjects, a Voronoi analysis of selected cones was performed in each of the patients, and metrics similar to those reported previously on photoreceptor mosaics were generated.[33,43–46] Contiguous sets of at least 100 cones were selected for analysis. The exact locations and the number of regions depended on where unambiguous, contiguous arrays of cones were best visualized. The relative SD of the Voronoi domain areas, the percentage of triangularly packed cones, and the relative SD of the number of Voronoi polygon sides were compared with those of healthy subjects.

RESULTS

Four unrelated patients with *peripherin/RDS* mutations ranged in age from 45 to 65 years. Family history included central vision loss in the sixth decade for the father and paternal aunt and in the third decade for 1 of the 3 sons of the paternal aunt of patient 1, and central vision loss in the fourth decade for the mother, one maternal aunt, and the maternal grandmother of patient 2. BCVA ranged from 20/20 to 5/100. Foveal sensitivities were reduced and ranged from 35 to 13 dB. Fundus examination revealed bilateral symmetric RPE mottling with focal RPE atrophy in patients 1, 2, and 4; the fovea was spared in all patients (Figs. 1–4A). AF showed diffuse heterogeneity throughout the macula in all the patients and virtual absence of AF in regions of RPE atrophy (Figs. 1–4B). Full-field ERG responses were normal
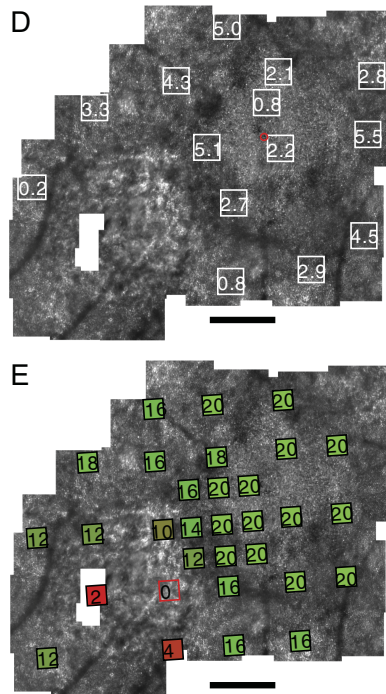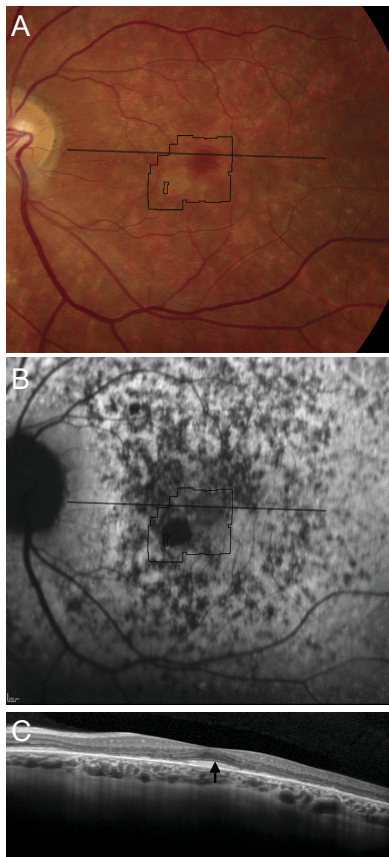
FIGURE 1. Fundus photograph (**A**) and AF (**B**) of patient 1 (Cys213Tyr) shows RPE mottling diffusely throughout the macula with regional atrophy inferonasal to fixation. (**A**, **B**, *black lines*) Region imaged with AOSLO and OCT, respectively. (**C**) OCT through fixation reveals outer nuclear, inner segment, and outer segment layer loss eccentric to a central region of relatively preserved outer retinal structures where highly reflective features are present in the outer segment/RPE junction layer (*arrow*). (**D**) High-resolution images of macular cone structure show cone spacing is contiguous around fixation but the spacing is generally increased with interspersed patches of normal spacing. *Red dot*: fixation. Fundus-guided microperimetry shows >2 log units sensitivity loss (indicated by 0) in a small atrophic region inferonasal to the fovea, 1 to 2 log units sensitivity loss in areas of heterogeneous AF, and normal sensitivity (indicated by 20 dB) within 0.5° of fixation (**E**). Scale bar = 1°.
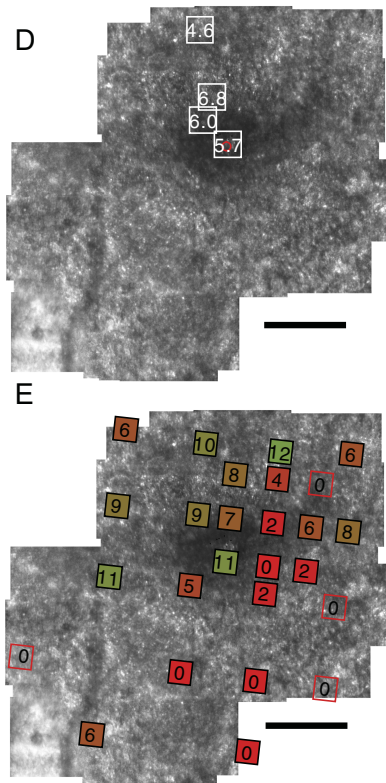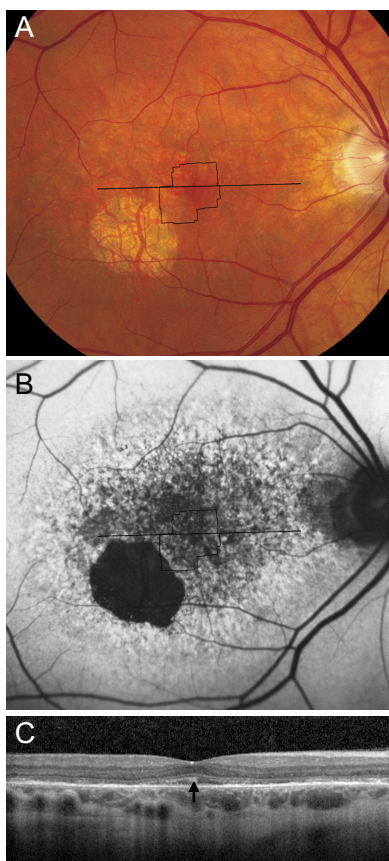
FIGURE 2. Fundus photograph (**A**) and AF (**B**) of patient 2 (Arg172Trp) shows RPE mottling diffusely throughout the macula with regional atrophy inferotemporal to fixation. (**A**, **B**, *black lines*) Region imaged with AOSLO and SD-OCT, respectively. (**C**) SD-OCT through fixation reveals outer nuclear, inner segment, and outer segment layer loss eccentric to a central region of relatively preserved outer retinal structures, where highly reflective features are present in the outer segment/RPE junction layer (*arrow*). (**D**) High-resolution images of macular cone structure show cone spacing is increased by 4.6 to 6.8 SD above the normal mean throughout the macula. *Red dot*: fixation. Fundus-guided microperimetry shows >2 log units sensitivity loss (indicated by 0) in regions of heterogeneous AF, with 1 to 2 log units sensitivity loss within 1° of fixation (**E**). A hyperreflective region with increased cone spacing (Z-score 5.7) was present at the fovea (see Fig. 6B, left). Scale bar, 1°.

in amplitude and timing in each eye of patients 2 and 3, but cone responses were reduced to a greater extent than rod responses in patient 1, and rod responses were severely reduced to a greater extent than cone responses in patient 4 (Table 1). Multifocal ERG response densities were moderately to severely reduced, with delayed timing in each patient (Table 1). OCT showed extensive loss of the outer nuclear, inner segment, and outer segment layers in the central macula. At the fovea, outer retinal structure was relatively preserved, but hyperreflective, irregular structures were present in the outer segment-RPE junction layer in all patients; however, this layer was least abnormal in patient 1, who had the best visual acuity and visual sensitivity of the patients despite having a cone-rod dystrophy phenotype based on full-field ERG testing (Figs. 1–4C, 5). Cone spacing was significantly increased from normal (Z-scores >5) in many regions through the central 4°, although cone spacing variation was heterogeneous and patches with normal cone spacing were interspersed with more sparsely packed cones (Figs. 1–4D). Furthermore, hyperreflective cones were observed adjacent to fixation in patients 2 and 3. Microperimetry showed reduced sensitivity by 1 to 2 log units throughout the central 8°, with best function in the central 2° surrounding the fovea (Figs. 1–4E). Genetic testing revealed heterozygous single nucleotide changes predicted to affect peripherin/RDS protein structure in the second intradiscal D2 domain in each patient (Table 1).

Contiguous patches of cones from each patient, averaging just over 100 cones per patch, were selected for Voronoi analysis. For comparison, five contiguous patches of cones at similar locations were selected from AOSLO images of three healthy eyes. Table 2 shows the results. A one-tailed *t*-test showed highly significant differences ($P < 0.001$) in the following metrics: relative SD (in %) of the area of the Voronoi patches and the relative SD (in %) of the number of sides of the Voronoi polygons. A one-tailed Mann–Whitney *U* test showed a highly significant difference ($P < 0.001$) in the percentage of six-sided polygons. These indicate that there is a disruption in normal cone packing associated with the increase in cone spacing. Figure 6 shows representative images of the cone mosaic in patient 2 with Voronoi polygon overlays.

The foveal AOSLO images and the OCT scans for all patients are shown at high magnification in Figure 5. CFS thickness was 233 μm in patient 1, 237 μm in patient 2, 217 μm in patient 3, and 231 μm in patient 4, all of which were significantly lower than the normal values. The minimum distance at the foveal depression between the inner limiting membrane and the external limiting membrane was measured manually and compared with normal data. The outer nuclear layer thickness at the fovea (normal, 116.1 $\pm$ 13.2 μm [mean $\pm$ 1 SD]) was within normal limits for all patients. The distance between the inner segment/outer segment junction and the basement membrane of the RPE-Bruch membrane complex at the fovea in each subject was within 1 SD of the normal mean (75.7 $\pm$ 4.9 μm; patient 1, 70 μm; patient 2, 77 μm; patient 3, 83 μm; patient 4, 59 μm). However, the outer segment-RPE junction layer showed increased reflectivity in all patients. The location of fixation for patients 2 and 3 coincided with the hyperreflective central region observed on both AOSLO and OCT images (Figs. 5B, 5C). Patient 4 used a reflective region of cones surrounded by regions of reduced reflectivity, and the outer segment-RPE junction layer was hyperreflective on OCT (Fig. 5D). The OCT indicated that the hyperreflectivity arose at the outer segment-RPE junction layer. Despite these changes, the cones remained functional and were used for fixation.

Figure 3. Fundus photograph (**A**) and AF (**B**) of patient 3 (Gly208Asp) shows RPE mottling diffusely throughout the macula. (**A**, **B**, *black lines*) Region imaged with AOSLO and SD-OCT, respectively. (**C**) SD-OCT through fixation reveals outer nuclear, inner segment, and outer segment layer loss eccentric to a central region of relatively preserved outer retinal structure, where highly reflective features are present in the outer segment/RPE junction layer (*arrow*). (**D**) High-resolution images of macular cone structure show cone spacing is irregular and normal (0.95 SD above the mean) in regions but increased by >5 SD above the mean in regions near the fovea. *Red dot*: fixation. Fundus-guided microperimetry shows >2 log units sensitivity loss (indicated by 0) in regions of heterogeneous AF, with 1 to 2 log units sensitivity loss within 1° of fixation (**E**). Hyperreflective cones are present at fixation (see Fig. 6C, left). Scale bar, 1°.
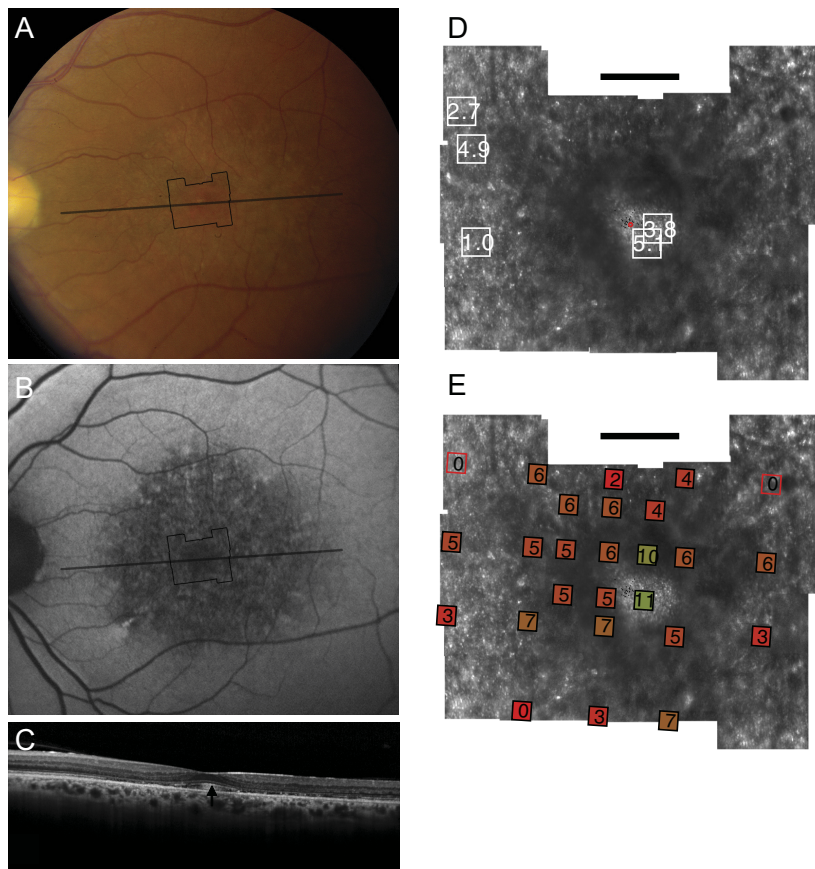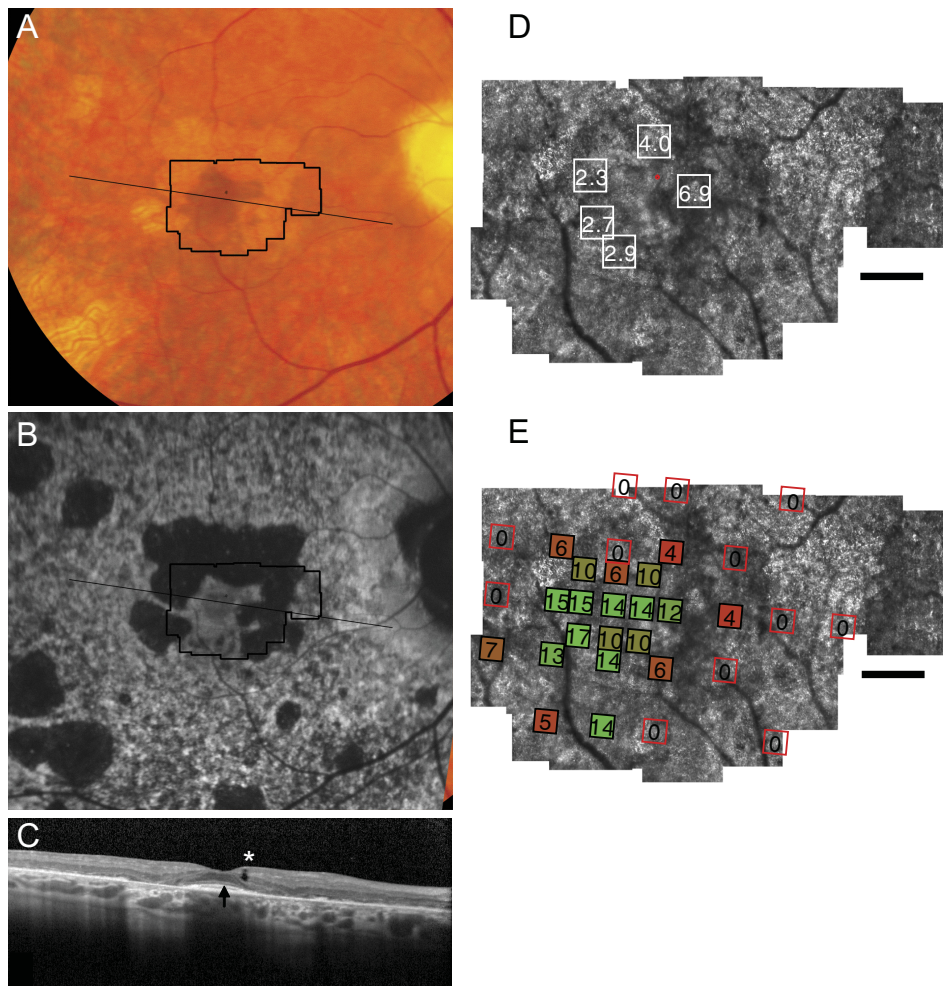
Figure 4. Fundus photograph (**A**) and AF (**B**) of patient 4 (Pro210Arg) shows RPE mottling diffusely throughout the macula, with atrophy surrounding fixation superiorly, nasally, and temporally. (**A**, **B**, *black lines*) Region imaged with AOSLO and SD-OCT, respectively. (**C**) SD-OCT through fixation reveals outer nuclear, inner segment, and outer segment layer loss eccentric to a central region of relatively preserved outer retinal structure, where highly reflective features are present in the outer segment/RPE junction layer (*arrow*) in addition to an inner retinal hyporeflective space (*asterisk*). (**D**) High-resolution images of macular cone structure show cone spacing is near normal at the fovea (2.27–2.94 SD greater than mean) but is more significantly increased in regions of reduced reflectivity nasal to the fovea (4.04–6.86 SD above mean). *Red dot*: fixation. Fundus-guided microperimetry shows >2 log units sensitivity loss (indicated by 0) in regions of atrophy seen on AF, with <1 log unit sensitivity loss within 1° of fixation (**E**). Scale bar, 1°.

Discussion

Using high-resolution imaging techniques, we observed the following features in a small number of unrelated patients with disease-causing mutations in the *peripherin/RDS* gene predicted to affect protein structure in the second intradiscal domain. In general, cone spacing was increased significantly throughout macular regions of irregular, heterogeneous AF; however, regions with normal cone spacing surrounded by regions of increased cone spacing were occasionally present (patient 3; Fig. 3D). In addition, cone packing was abnormal throughout regions of heterogeneous AF, demonstrated with Voronoi analysis (Fig. 6; Table 2). Visual sensitivity was reduced in most regions with heterogeneous AF, though visual acuity was well preserved and sensitivity was normal near the fovea in patient 1. OCT measures of retinal thickness demonstrated diffuse loss of outer retinal structures extending from 0.5° eccentricity, with relative preservation of the outer nuclear and inner segment layers at the fovea corresponding to reduced CFS thickness in the study patients compared with healthy subjects. At the fovea, the outer segment and the RPE layers showed hyperreflective profiles; these changes were least pronounced in patient 1, who demonstrated diffuse cone dysfunction on full-field ERG testing, consistent with primary cone degeneration.

These findings suggest that in patients with *peripherin/RDS*–associated retinal degeneration, foveal photoreceptor structure and function are preserved within macular regions of increased cone spacing and outer retinal degeneration. Local factors contributing to the observed regional intramacular variability could include differential accumulation of lipofuscin in RPE cells, increased melanin in foveal RPE cells, a protective function of macular pigment, or the lack of rod photoreceptors at the fovea. Our findings suggest that although peripherin/RDS is critical for rod and cone outer segment structure throughout the retina, photoreceptor survival is determined locally by regional factors. This hypothesis is supported by previous reports of greater pericentral than peripheral dysfunction and normal phototransduction in patients with heterozygous mutations in *peripherin/RDS* associated with retinal degeneration.[15,47] In addition, mice with heterozygous mutations in *rds* show retention of cone cell nuclei in the central retina more frequently than rod cell nuclei.[48] Our findings suggest that foveal cones may be resistant to photoreceptor degeneration caused by *peripherin/RDS* mutations, perhaps implicating local factors such as RPE melanin, lipofuscin accumulation, or macular pigment in the pathogenesis of *peripherin/RDS*-associated retinal degeneration. Future studies on macular pigment in patients with in *peripherin/RDS*-associated retinal degeneration may help distinguish between these alternative hypotheses.

The foveal sparing observed in patients with *peripherin/RDS*-associated retinal degeneration makes visual acuity a poor measure of disease severity and progression. The four patients in the present study had variable degrees of disease severity, ranging from localized macular abnormalities in AF and sensitivity in patient 3 to diffuse photoreceptor dysfunction in
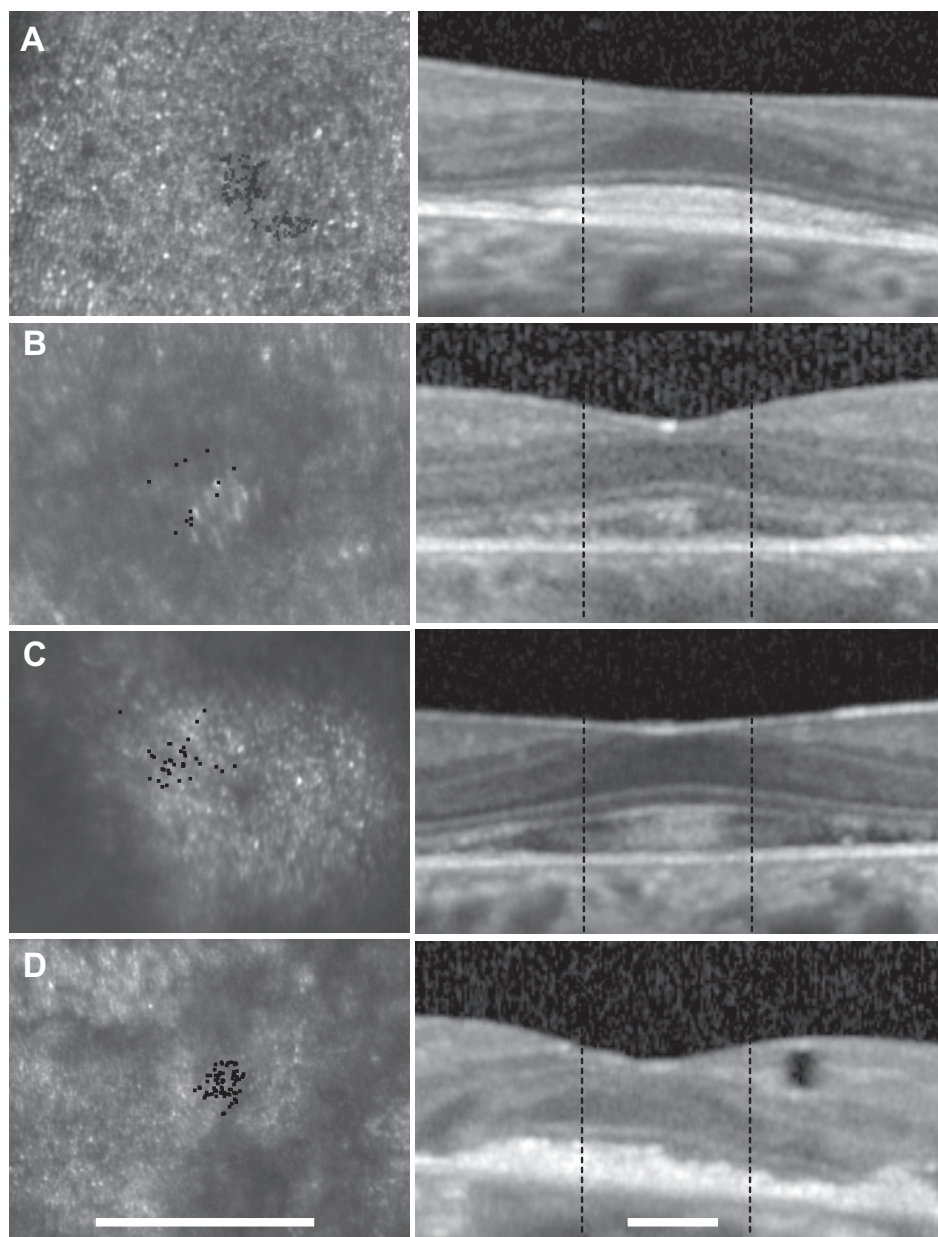
FIGURE 5. *Left*: magnified section of AOSLO image for each patient around the fixation point (*black dots*). Patients 2 and 3 use a region of hyperreflective cones for fixation, whereas fixation is located between two highly reflective regions in patient 4. *Right*: horizontal OCT scans through fixation. Outer retinal structures are relatively preserved at the fovea, but the outer nuclear layer is thin, and the outer segments/RPE junction layer is hyperreflective and elongated in patients 2 to 4 (**B–D**). The outer segments in patient 1 (who had evidence of diffuse cone dysfunction and the best visual acuity and sensitivity) were the least elongated and hyperreflective (**A**, *right*). Scale bars, 0.67°.

patients 1 and 4, but vision was at least 20/30 in at least one eye in all patients. More sensitive indices of disease severity and progression might include foveal or macular sensitivity, color vision, and macular structural measures such as OCT and AOSLO. Foveal preservation may make *peripherin/RDS*-associated retinal degeneration an attractive candidate for neuroprotective therapies designed to slow disease progression.[49] Clinical trials designed to measure response to experimental therapies may have to study nontraditional outcome measures, including foveal and macular sensitivity and high-resolution structural measures such as those presented here, to most precisely measure safety and efficacy in patients with *peripherin/RDS*-associated retinal degeneration because visual acuity is likely to be an insensitive measure in this patient population.

The relationship between hyperreflective cone profiles on both OCT and AOSLO in regions of preserved visual function at or near fixation is worthy of longitudinal study. Perhaps cones progress from normal heterogenous reflective profiles to a

diseased state with irregular inner segment/outer segment junction and outer segment/RPE junction layers on SD-OCT, where cones retain function but show increased reflectivity. Progressive degeneration may be associated with reduced reflectivity associated with reduced sensitivity and increased cone spacing, as observed in patient 4 in regions where unambiguous cones were visualized adjacent to regions of RPE atrophy (Fig. 4D).

Some features of clinical retinal degeneration associated with *peripherin/RDS* mutations suggest there are similarities to the rds± mouse model, in which the peripherin/RDS heterozygote has unstable disc structure, altered disc shedding, and large phagosomes in the RPE that lead to secondary RPE changes and fundus abnormalities.[15,50] In the present study, irregular profiles were observed in the outer segment/RPE junction layer throughout the macula and especially at the fovea in all patients (Figs. 1–4C). These hyperreflective profiles were associated with an irregular, disrupted appearance to the

TABLE 2. Voronoi Analysis Results

	Eccentricity (°)	Average Area (arcmin²)	Area SD (%)	Six-Sided Polygons (%)	Sides SD (n)
Healthy 1	0.95 ST	0.78	10.3	57	11.6
	1.1 N	0.73	10.1	79	8.2
	1.52 N	0.92	12.2	64	10
	1.6 I	1.18	8.7	55	12.2
	2.75 IT	1.7	13.2	50	13.5
Healthy 2	0.67 IT	0.78	15.5	61	11
	0.67 S	0.95	14.8	56	11.6
	1.19 N	1.12	11.8	60	11.7
	1.55 N	1.32	13.1	64	10.8
	2.25 SN	1.92	11	64	10.3
Healthy 3	0.78 I	0.66	11.9	78	8.4
	0.89 N	0.77	13	68	10.8
	1.27 T	1	13.8	63	10.7
	1.67 T	1.16	10.7	63	11
	1.75 IT	1.23	11.2	57	12.3
	Average		12.1	62.6	10.9
	SD		1.8	7.9	1.4
Patient 1	0.81 N	1.35	18.9	38	15
	1.26 T	1.45	15.2	51	10.3
	2.87 SN	2.74	22.4	33	13.8
Patient 2	0.48 ST	1.52	19.9	45	15.9
	0.67 S	1.75	19.6	41	14.7
Patient 3	2.30 N	2.01	17.5	40	14.6
	0.12 fovea	1.24	25.7	50	13.6
Patient 4	1.23 IT	1.44	18.6	58	11.9
	1.37 IT	1.44	20.7	42	15
	Average		19.8	44.2	13.9
	SD		3.0	7.6	1.8
			*P < 0.001	*P < 0.001	*P < 0.001

Contiguous sets of ~100 cones were selected for analysis. The top three sets are from normal healthy eyes, and the lower four sets are from the four patients. SNIT refers to superior, nasal, inferior, and temporal retinal directions. In patients with *peripherin/RDS* mutations, the SD of the Voronoi domain area is greater, the percentage of six-sided polygons is lower, and the SD of the number of sides is greater. *P* values are listed on the lowest row of the table.

outer segment/RPE junction layer within several degrees of the fovea in the macula of each patient. A similar pattern of disrupted inner segment/outer segment layers with foveal preservation was reported by Godara et al[34] in a patient with fundus AF characteristics similar to those observed in patients with mutations in *peripherin/RDS*, although molecular characterization of the *peripherin/RDS* gene was not described in that study. The irregular outer segment layer observed in the present study may represent the human analog of the abnormal outer segment whorl-like structures reported in mice with heterozygous mutations in *peripherin/RDS*[48] and transgenic mice expressing a proline-216-leucine substitution in peripherin/RDS.[51] The outer segment/RPE junction layer abnormalities may be attributed to abnormal intracellular interactions or abnormal interactions with the extracellular matrix. In addition, the hyperreflective outer segment/RPE junction layer and cone profiles observed with OCT and AOSLO may represent light wave-guided by cones overlying RPE cells with enlarged phagosomes containing shed abnormal disc outer segments, as have been observed in rds± mice,[48] or RPE cells engorged with lipofuscin deposits, as reported in a histopathological study of a patient with pattern dystrophy caused by the Cys213Tyr mutation as in patient 1 in the present study.[4] Perhaps enlarged phagosomes or lipofuscin increase scattered light from RPE cells, with secondary increased wave-guiding of overlying cone inner segments. The present study provides functional correlates to the observation of outer segment abnormalities caused by *peripherin/RDS* mutations; hyperreflective, abnormal outer segments retain useful function at the fovea, though sensitivity is reduced in association with irregu-lar, disrupted outer segment/RPE junction layer profiles in the macula outside the foveal center.

Light and electron microscopic analysis of a retina from a patient with the Cys213Tyr *peripherin/RDS* mutation showed RPE cells distended with lipofuscin and melano-lipofuscin associated with disrupted outer segments and abrupt transition between areas of photoreceptor and RPE atrophy and relatively intact retina.[4] Immunohistochemical and electron microscopic evaluation of the peripheral retina of a patient with the R172W *peripherin/RDS* mutation showed reduced outer segment length and density and dysplastic outer segments with discs distorted into whorl-like structures.[52] A clinicopathological study of a patient whose family was subsequently found to carry the P210R mutation showed focal loss of retinal photoreceptors and pigment migration into the retina with clumping of pigment-laden cells and chorioretinal adhesion at the fovea and paracentral thinning of the pigment epithelium.[53] No histologic studies have been reported from patients with maculopathies caused by the G208D *peripherin/RDS* mutations.

Histopathologic specimens studied ex vivo preclude accurate correlation between macular cone structure and function. Measures of outer retinal structure and function on a localized scale, such as that presented in the present study, provide critical insight into the effect of *peripherin/RDS* mutations on macular photoreceptors and demonstrate significant regional variation within the maculae of affected patients. These findings may yield insight into local factors that affect photoreceptor resistance or sensitivity to degeneration in patients with mutations in *peripherin/RDS*.
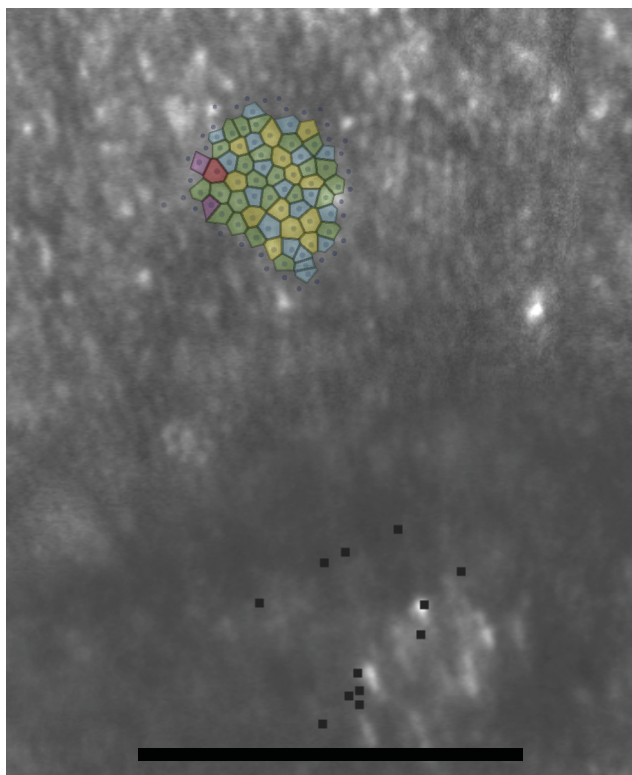
FIGURE 6. Voronoi domains superimposed on the cones for patient 2. The polygons are color-coded by the number of sides (*red*, 8; *yellow*, 7; *green*, 6; *blue*, 5; *purple*, 4). *Black dots*: PRL (see Fig. 5). Scale bar, 0.5°.

References

1. Goldberg AF, Ritter LM, Khattree N, et al. An intramembrane glutamic acid governs peripherin/rds function for photoreceptor disk morphogenesis. *Invest Ophthalmol Vis Sci.* 2007;48:2975–2986.

2. Farrar GJ, Jordan SA, Kenna P, et al. Autosomal dominant retinitis pigmentosa: localization of a disease gene (*RP6*) to the short arm of chromosome 6. *Genomics.* 1991;11:870–874.

3. Kajiwara K, Hahn LB, Mukai S, Travis GH, Berson EL, Dryja TP. Mutations in the human retinal degeneration slow gene in autosomal dominant retinitis pigmentosa. *Nature.* 1991;354:480–483.

4. Zhang K, Garibaldi DC, Li Y, Green WR, Zack DJ. Butterfly-shaped pattern dystrophy: a genetic, clinical, and histopathological report. *Arch Ophthalmol.* 2002;120:485–490.

5. Francis PJ, Schultz DW, Gregory AM, et al. Genetic and phenotypic heterogeneity in pattern dystrophy. *Br J Ophthalmol.* 2005;89:1115–1119.

6. Michaelides M, Holder GE, Bradshaw K, Hunt DM, Moore AT. Cone-rod dystrophy, intrafamilial variability, and incomplete penetrance associated with the R172W mutation in the peripherin/RDS gene. *Ophthalmology.* 2005;112:1592–1598.

7. Felbor U, Schilling H, Weber BH. Adult vitelliform macular dystrophy is frequently associated with mutations in the peripherin/RDS gene. *Hum Mutat.* 1997;10:301–309.

8. Keilhauer CN, Meigen T, Stohr H, Weber BH. Late-onset central areolar choroidal dystrophy caused by a heterozygous frame-shift mutation affecting codon 307 of the peripherin/RDS gene. *Ophthalmic Genet.* 2006;27:139–144.

9. Keilhauer CN, Meigen T, Weber BH. Clinical findings in a multigeneration family with autosomal dominant central areolar choroidal dystrophy associated with an Arg195Leu mutation in the peripherin/RDS gene. *Arch Ophthalmol.* 2006;124:1020–1027.

10. Gamundi MJ, Hernan I, Muntanyola M, et al. High prevalence of mutations in peripherin/RDS in autosomal dominant macular dystrophies in a Spanish population. *Mol Vis.* 2007;13:1031–1037.

11. Dryja TP, Hahn LB, Kajiwara K, Berson EL. Dominant and digenic mutations in the peripherin/RDS and ROM1 genes in retinitis pigmentosa. *Invest Ophthalmol Vis Sci.* 1997;38:1972–1982.

12. Kedzierski W, Weng J, Travis GH. Analysis of the rds/peripherin.rom1 complex in transgenic photoreceptors that express a chimeric protein. *J Biol Chem.* 1999;274:29181–29187.

13. Kohl S, Christ-Adler M, Apfelstedt-Sylla E, et al. RDS/peripherin gene mutations are frequent causes of central retinal dystrophies. *J Med Genet.* 1997;34:620–626.

14. Piguet B, Heon E, Munier FL, et al. Full characterization of the maculopathy associated with an Arg-172-Trp mutation in the RDS/peripherin gene. *Ophthalmic Genet.* 1996;17:175–186.

15. Wells J, Wroblewski J, Keen J, et al. Mutations in the human retinal degeneration slow (RDS) gene can cause either retinitis pigmentosa or macular dystrophy. *Nat Genet.* 1993;3:213–218.

16. Wroblewski JJ, Wells JA 3rd, Eckstein A, et al. Macular dystrophy associated with mutations at codon 172 in the human retinal degeneration slow gene. *Ophthalmology.* 1994;101:12–22.

17. Nakazawa M, Wada Y, Tamai M. Macular dystrophy associated with monogenic Arg172Trp mutation of the peripherin/RDS gene in a Japanese family. *Retina.* 1995;15:518–523.

18. Reig C, Serra A, Gean E, et al. A point mutation in the RDS-peripherin gene in a Spanish family with central areolar choroidal dystrophy. *Ophthalmic Genet.* 1995;16:39–44.

19. Donoso LA, Hageman G, Frost A, et al. Autosomal dominant macular dystrophy in a large Canadian family. *Can J Ophthalmol.* 2003;38:33–40.

20. Downes SM, Fitzke FW, Holder GE, et al. Clinical features of codon 172 RDS macular dystrophy: similar phenotype in 12 families. *Arch Ophthalmol.* 1999;117:1373–1383.

21. Payne AM, Downes SM, Bessant DA, Bird AC, Bhattacharya SS. Founder effect, seen in the British population, of the 172 peripherin/RDS mutation-and further refinement of genetic positioning of the peripherin/RDS gene. *Am J Hum Genet.* 1998;62:192–195.

22. Cideciyan AV. In vivo assessment of photoreceptor function in human diseases caused by photoreceptor-specific gene mutations. *Methods Enzymol.* 2000;316:611–626.

23. Sohocki MM, Daiger SP, Bowne SJ, et al. Prevalence of mutations causing retinitis pigmentosa and other inherited retinopathies. *Hum Mutat.* 2001;17:42–51.

24. Trujillo MJ, Bueno J, Osorio A, et al. Three novel RDS-peripherin mutations (689delT, 857del17, G208D) in Spanish families affected with autosomal dominant retinal degenerations. Mutations in brief no. 147. Online. *Hum Mutat.* 1998;12:70.

25. Trujillo MJ, Martinez-Gimeno M, Gimenez A, et al. Two novel mutations (Y141H; C214Y) and previously published mutation (R142W) in the RDS-peripherin gene in autosomal dominant macular dystrophies in Spanish families. *Hum Mutat.* 2001;17:80.

26. Feist RM, White MF Jr, Skalka H, Stone EM. Choroidal neovascularization in a patient with adult foveomacular dystrophy and a mutation in the retinal degeneration slow gene (Pro 210 Arg). *Am J Ophthalmol.* 1994;118:259–260.

27. Gorin MB, Jackson KE, Ferrell RE, et al. A peripherin/retinal degeneration slow mutation (Pro-210-Arg) associated with macular and peripheral retinal degeneration. *Ophthalmology.* 1995;102:246–255.

28. Romero-Borja F, Venkateswaran K, Roorda A, Hebert T. Optical slicing of human retinal tissue in vivo with the adaptive optics scanning laser ophthalmoscope. *Appl Opt.* 2005;44:4032–4040.

29. Roorda A, Williams DR. Optical fiber properties of individual human cones. *J Vision.* 2002;2:404–412.

30. Zhang Y, Roorda A. Evaluating the lateral resolution of the adaptive optics scanning laser ophthalmoscope. *J Biomed Opt.* 2006;11:014002.

31. Zhang Y, Poonja S, Roorda A. MEMS-based adaptive optics scanning laser ophthalmoscopy. *Opt Lett.* 2006;31:1268–1270.

32. Duncan JL, Zhang Y, Gandhi J, et al. High-resolution imaging with adaptive optics in patients with inherited retinal degeneration. *Invest Ophthalmol Vis Sci.* 2007;48:3283–3291.

33. Yoon MK, Roorda A, Zhang Y, et al. Adaptive optics scanning laser ophthalmoscopy images in a family with the mitochondrial DNA T8993C mutation. *Invest Ophthalmol Vis Sci.* 2009;50:1838–1847.

34. Godara P, Rha J, Tait DM, et al. Unusual adaptive optics findings in a patient with bilateral maculopathy. *Arch Ophthalmol.* 2010;128:253–254.

35. Rha J, Dubis AM, Wagner-Schuman M, et al. Spectral domain optical coherence tomography and adaptive optics: imaging photoreceptor layer morphology to interpret preclinical phenotypes. *Adv Exp Med Biol.* 2010;664:309–316.

36. Roorda A, Zhang Y, Duncan JL. High-resolution in vivo imaging of the RPE mosaic in eyes with retinal disease. *Invest Ophthalmol Vis Sci.* 2007;48:2297–2303.

37. Wolfing JI, Chung M, Carroll J, Roorda A, Williams DR. High-resolution retinal imaging of cone-rod dystrophy. *Ophthalmology.* 2006;113:1019 e1011.

38. Choi SS, Doble N, Hardy JL, et al. In vivo imaging of the photoreceptor mosaic in retinal dystrophies and correlations with visual function. *Invest Ophthalmol Vis Sci.* 2006;47:2080–2092.

39. Bowman KJ. A method for quantitative scoring of the Farnsworth Panel D-15. *Acta Ophthalmol (Copenh).* 1982;60:907–916.

40. Lanthony P. [Evaluation of the desaturated Panel D-15, I: method of quantification and normal scores]. *J Fr Ophtalmol.* 1986;9:843–847.

41. Marmor MF, Holder GE, Seeliger MW, Yamamoto S. Standard for clinical electroretinography (2004 update). *Doc Ophthalmol.* 2004;108:107–114.

42. Roorda A, Metha AB, Lennie P, Williams DR. Packing arrangement of the three cone classes in primate retina. *Vision Res.* 2001;41:1291–1306.

43. Baraas RC, Carroll J, Gunther KL, et al. Adaptive optics retinal imaging reveals S-cone dystrophy in tritan color-vision deficiency. *J Opt Soc Am A Opt Image Sci Vis.* 2007;24:1438–1447.

44. Galli-Resta L, Novelli E, Kryger Z, Jacobs GH, Reese BE. Modelling the mosaic organization of rod and cone photoreceptors with a minimal-spacing rule. *Eur J Neurosci.* 1999;11:1461–1469.

45. Li KY, Roorda A. Automated identification of cone photoreceptors in adaptive optics retinal images. *J Opt Soc Am A Opt Image Sci Vis.* 2007;24:1358–1363.

46. Shapiro MB, Schein SJ, de Monasterio FM. Regularity and structure of the spatial pattern of the blue cones of Macaque retina. *J Am Stat Assn.* 1985;803–814.

47. Jacobson SG, Cideciyan AV, Kemp CM, Sheffield VC, Stone EM. Photoreceptor function in heterozygotes with insertion or deletion mutations in the RDS gene. *Invest Ophthalmol Vis Sci.* 1996;37:1662–1674.

48. Hawkins RK, Jansen HG, Sanyal S. Development and degeneration of retina in rds mutant mice: photoreceptor abnormalities in the heterozygotes. *Exp Eye Res.* 1985;41:701–720.

49. Sieving PA, Caruso RC, Tao W, et al. Ciliary neurotrophic factor (CNTF) for human retinal degeneration: phase I trial of CNTF delivered by encapsulated cell intraocular implants. *Proc Natl Acad Sci U S A.* 2006;103:3896–3901.

50. Bird AC. Retinal photoreceptor dystrophies, LI: Edward Jackson Memorial Lecture. *Am J Ophthalmol.* 1995;119:543–562.

51. Kedzierski W, Lloyd M, Birch DG, Bok D, Travis GH. Generation and analysis of transgenic mice expressing P216L-substituted rds/peripherin in rod photoreceptors. *Invest Ophthalmol Vis Sci.* 1997;38:498–509.

52. Wickham LJ, Chen FK, Lewis GP, et al. Clinicopathological case series of four patients with inherited macular disease. *Invest Ophthalmol Vis Sci.* 2009;50:3553–3561.

53. Gass JD. A clinicopathologic study of a peculiar foveomacular dystrophy. *Trans Am Ophthalmol Soc.* 1974;72:139–156.